

## Supporting Information

# Tunable Magnetic Order in Two-dimensional Layered GdGe<sub>2</sub>

*Yuwan Wang,<sup>1</sup> Zichun Cui,<sup>1</sup> Hanghang Zeng,<sup>1</sup> Zijie Wang,<sup>2</sup> Xian Zhang,<sup>1</sup> Junqin Shi,<sup>1</sup> Tengfei Cao,<sup>1</sup>  
Xiaoli Fan<sup>1\*</sup>*

<sup>1</sup> State Key Laboratory of Solidification Processing, Center for advanced lubrication and seal  
Materials, School of Materials Science and Engineering, Northwestern Polytechnical University,  
127 YouYi Western Road, Xi'an, Shaanxi 710072, China

<sup>2</sup>School of Materials Science and Engineering, Xi'an Jiaotong University, 28 Xianning West Road,  
Xi'an, Shaanxi, 710049 China

\*Corresponding author: [xlfan@nwpu.edu.cn](mailto:xlfan@nwpu.edu.cn)

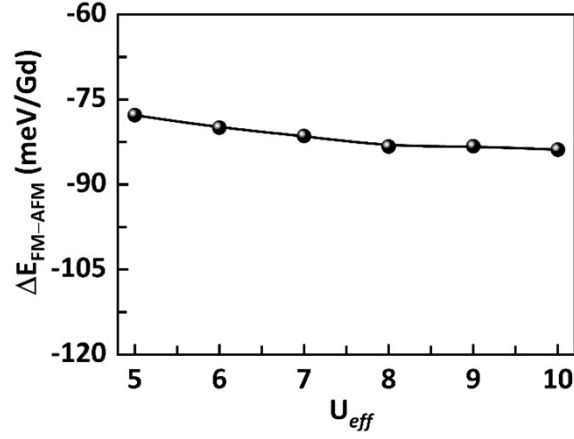


**Figure S1.** Energy difference between the ferromagnetic (FM) and anti-ferromagnetic (AFM) states of monolayer GdGe<sub>2</sub> calculated with different  $U_{eff}$ .

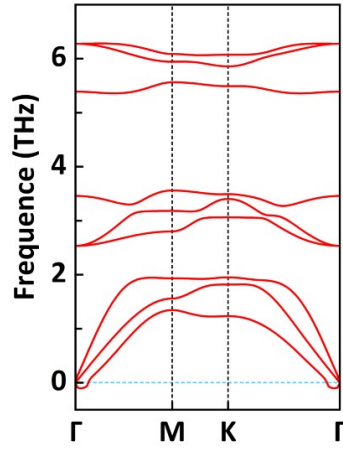


**Figure S2.** Phonon dispersion of GdGe<sub>2</sub> monolayer in the high-symmetry directions of the Brillouin zone.

The function relationships of Young's modulus ( $Y_{2D}$ ) and Poisson's ratio ( $\nu$ ) with polar angle ( $\varphi$ ) are as following:

$$Y_{2D}(\varphi) = \frac{C_{11}C_{22} - C_{12}^2}{C_{11}s^2 + C_{22}c^4 + \left(\frac{C_{11}C_{22} - C_{12}^2}{C_{66}} - 2C_{12}\right)c^2s^2}$$

$$\nu(\varphi) = \frac{\left(C_{11} + C_{22} - \frac{C_{11}C_{22} - C_{12}^2}{C_{66}}\right)c^2s^2 - C_{12}(s^4 + c^4)}{C_{11}s^2 + C_{22}c^4 + \left(\frac{C_{11}C_{22} - C_{12}^2}{C_{66}} - 2C_{12}\right)c^2s^2}$$

where  $\varphi$  is the polar angle relative to the x-axis,  $s$  and  $c$  are  $\sin\varphi$  and  $\cos\varphi$ , respectively.

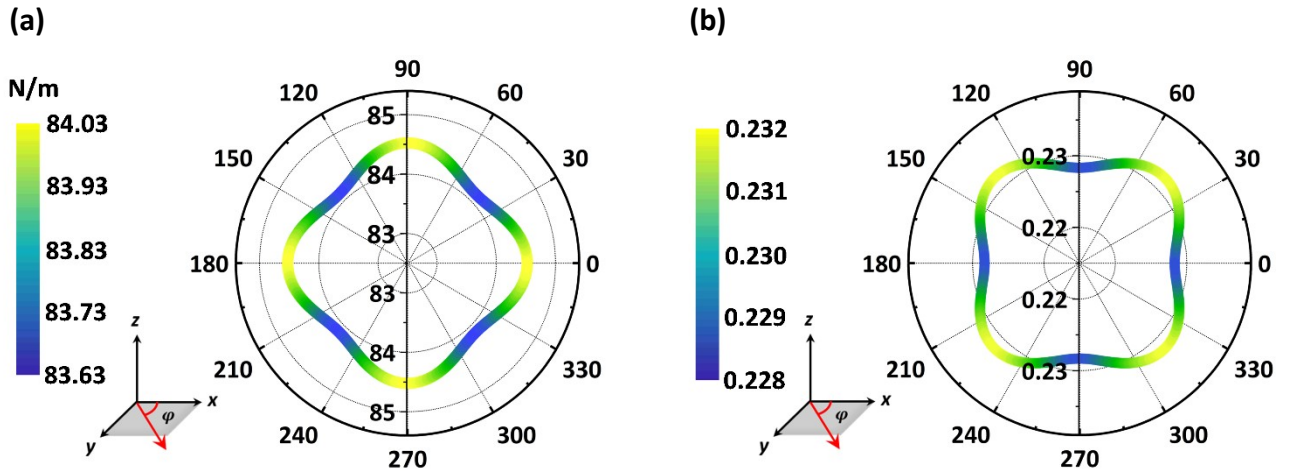


**Figure S3.** The evolution of (a) Young's modulus and (b) Poisson's ratio with respect to the polar angle ( $\varphi$ ) for monolayer  $\text{GdGe}_2$ .

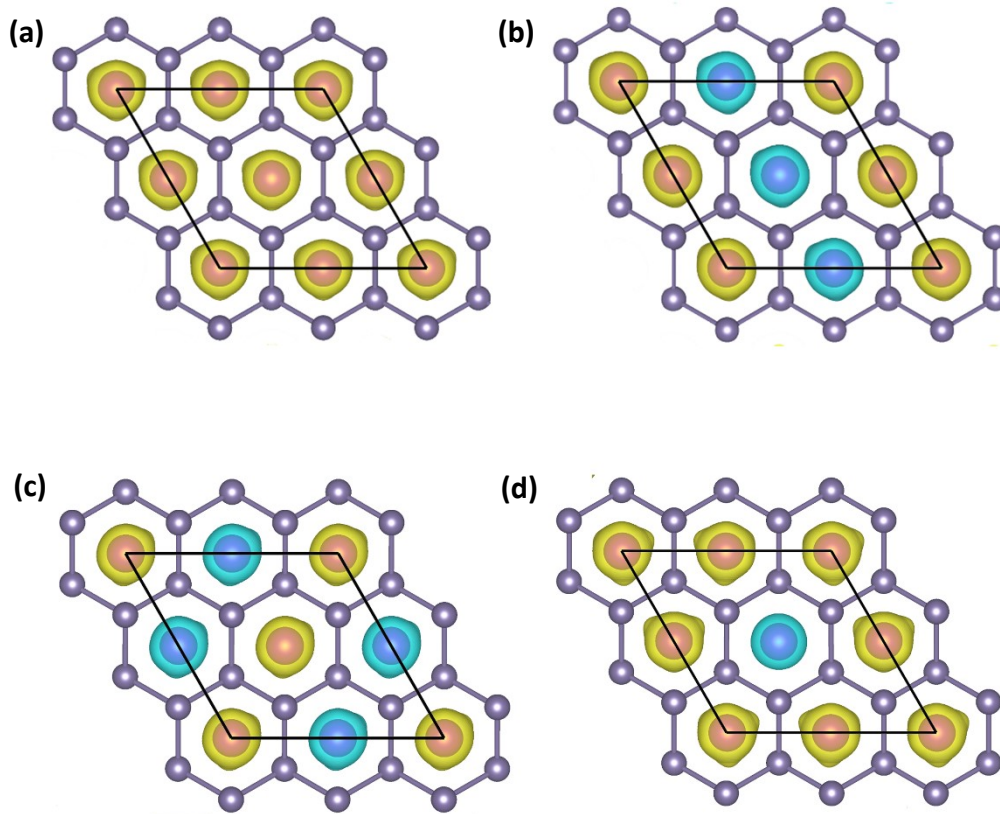


**Figure S4.** Spin-resolved charge density of  $\text{GdGe}_2$  monolayer in (a) ferromagnetic (FM), two anti-ferromagnetic (AFM), (b) G-AFM, (c) C-AFM, and (d) ferrimagnetic (FIM) configurations, respectively. The yellow and cyan colors represent the spin-up and spin-down charge, respectively. The isosurface value is set as  $0.008 \text{ e \AA}^{-3}$ .

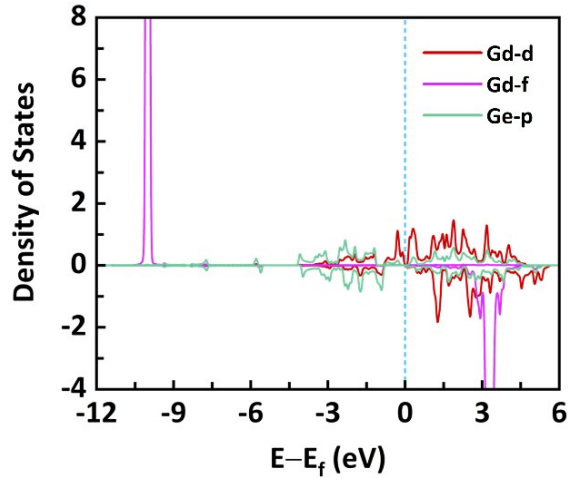


**Figure S5.** Orbital-resolved projected density of states of Gd and Ge atoms for monolayer  $\text{GdGe}_2$  calculated by PBE+U method.

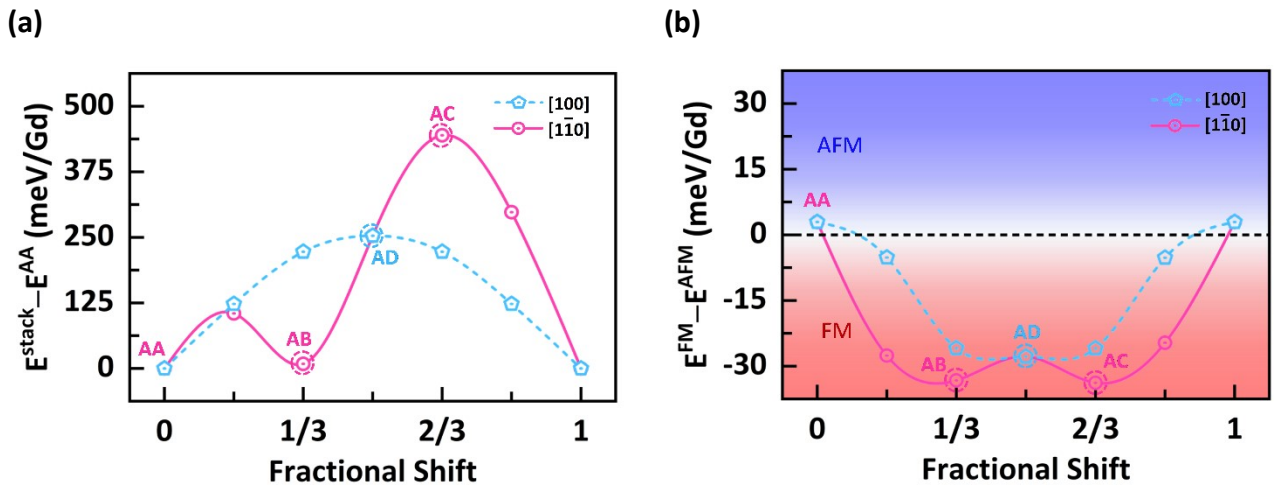


**Figure S6.** (a) Evolution of the interlayer stacking energy and (b) the interlayer exchange energy of bilayer  $\text{GdGe}_2$  with respect to the relative displacement of one layer to the other along high-symmetry  $[100]$  and  $[1\bar{1}0]$  directions after stacking-constraint atomic relaxation. Positive (negative) value in (b) represents the anti-ferromagnetic (AFM) (ferromagnetic, FM) interlayer exchange interaction.

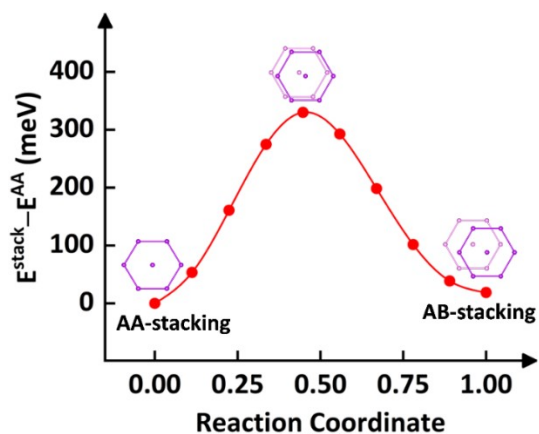


**Figure S7.** Minimum energy path for the stacking order transition between AA-stacking and AB-stacking bilayer  $\text{GdGe}_2$  calculated by CI-NEB method.

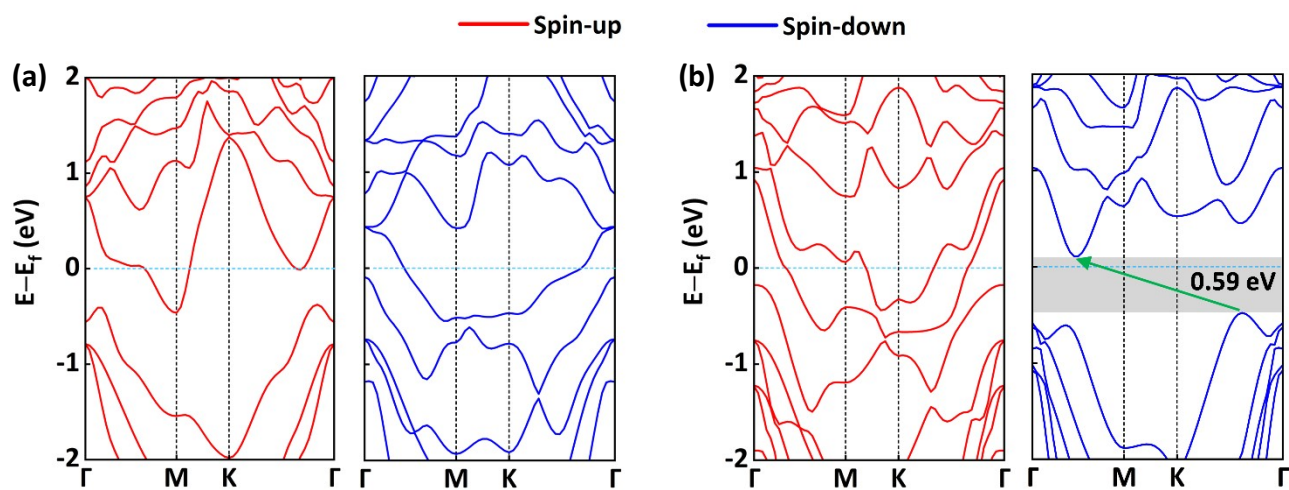


**Figure S8.** Spin-resolved band structures of (a) AA-stacking and (b) AB-stacking bilayer  $\text{GdGe}_2$  calculated by HSE06 method.

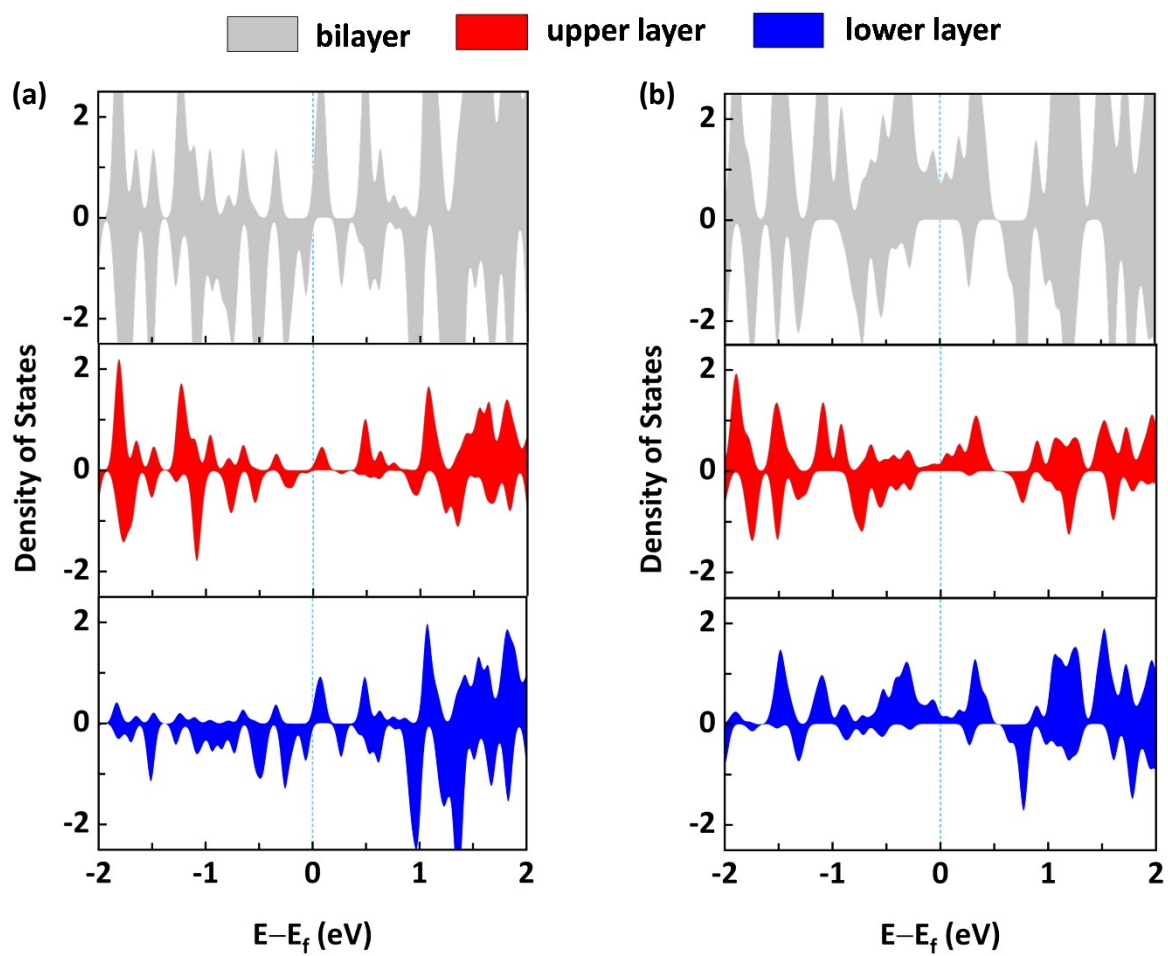


**Figure S9.** The total density of states and layer-resolved partial density of states for (a) AA- and (b) AB-stacking bilayer GdGe<sub>2</sub>.

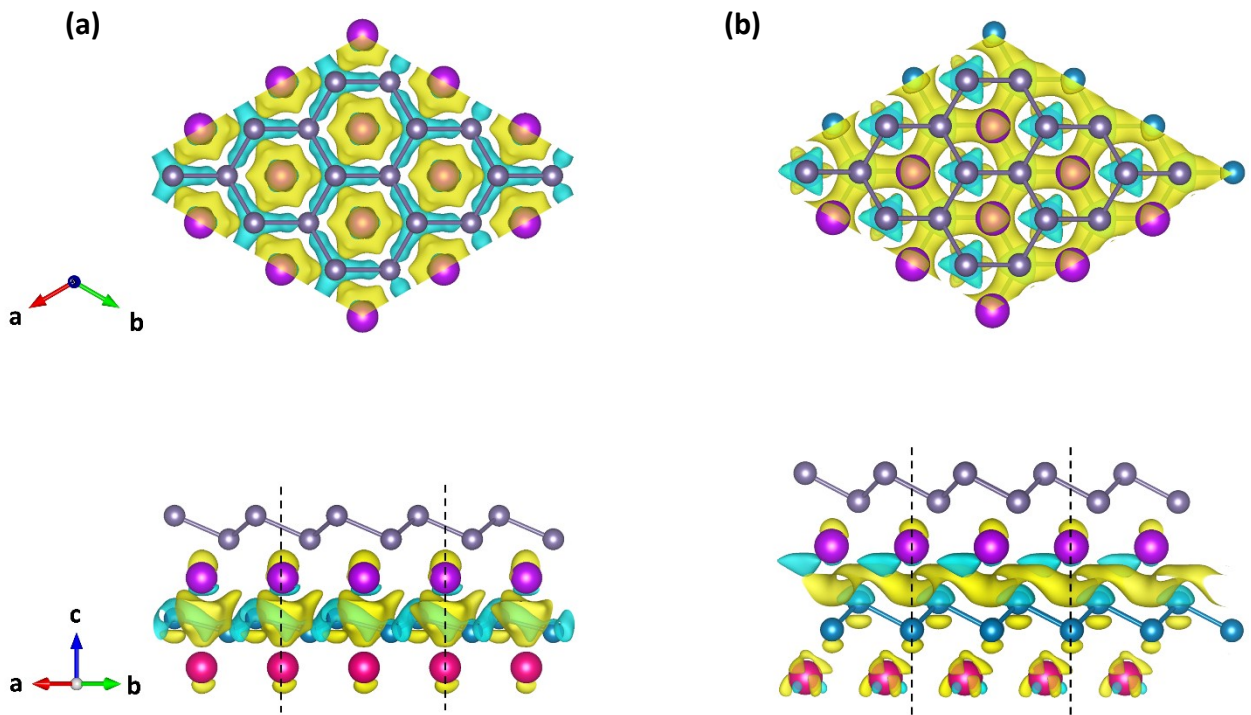


**Figure S10.** Top and side views of differential charge density for (a) AA-stacking and (b) AB-stacking bilayer  $\text{GdGe}_2$ . The isosurface value is set as  $0.002 \text{ e } \text{\AA}^{-3}$ . The yellow and cyan colors represented the charge accumulation and depletion, respectively.

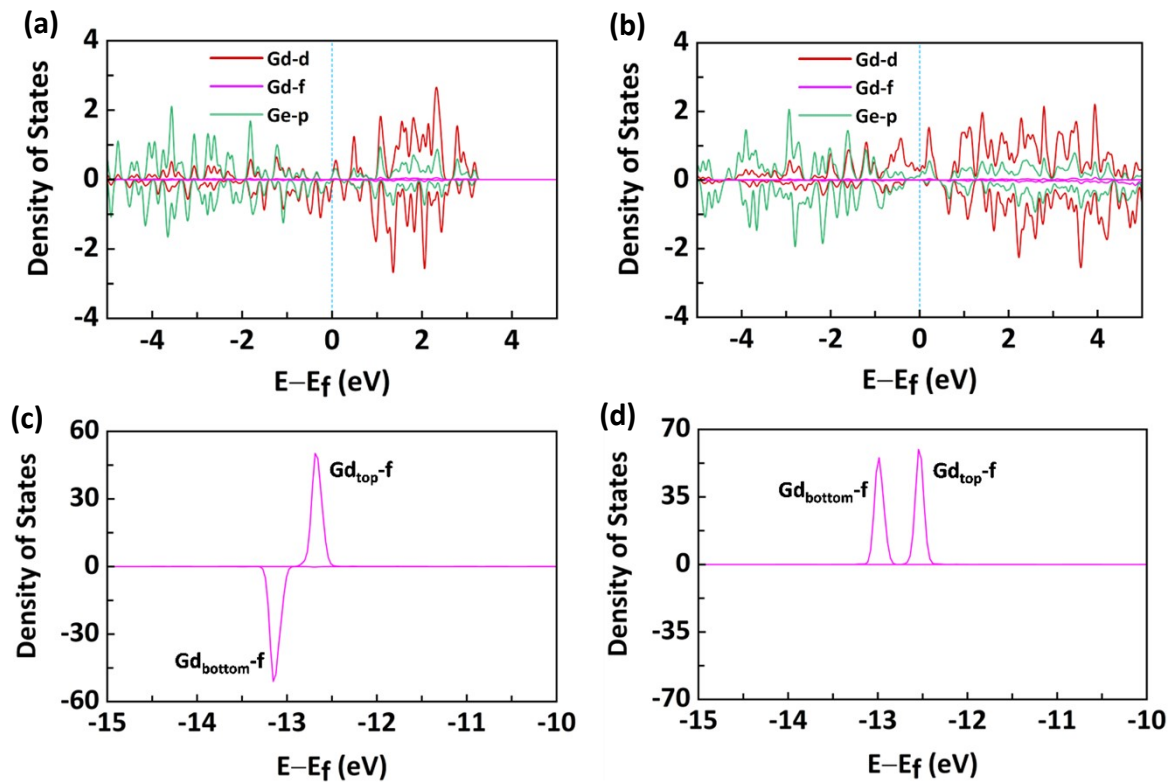


**Figure S11.** Orbital-resolved projected density of states of Gd and Ge atoms in (a) AA-stacking and (b) AB-stacking bilayer GdGe<sub>2</sub> calculated by HSE06 method. The distribution of Gd-f orbitals in (c) AA-stacking and (d) AB-stacking bilayer GdGe<sub>2</sub> calculated by HSE06 method. Gd<sub>top</sub> (Gd<sub>bottom</sub>) represents the Gd atoms of top (bottom) layer in bilayer GdGe<sub>2</sub>.



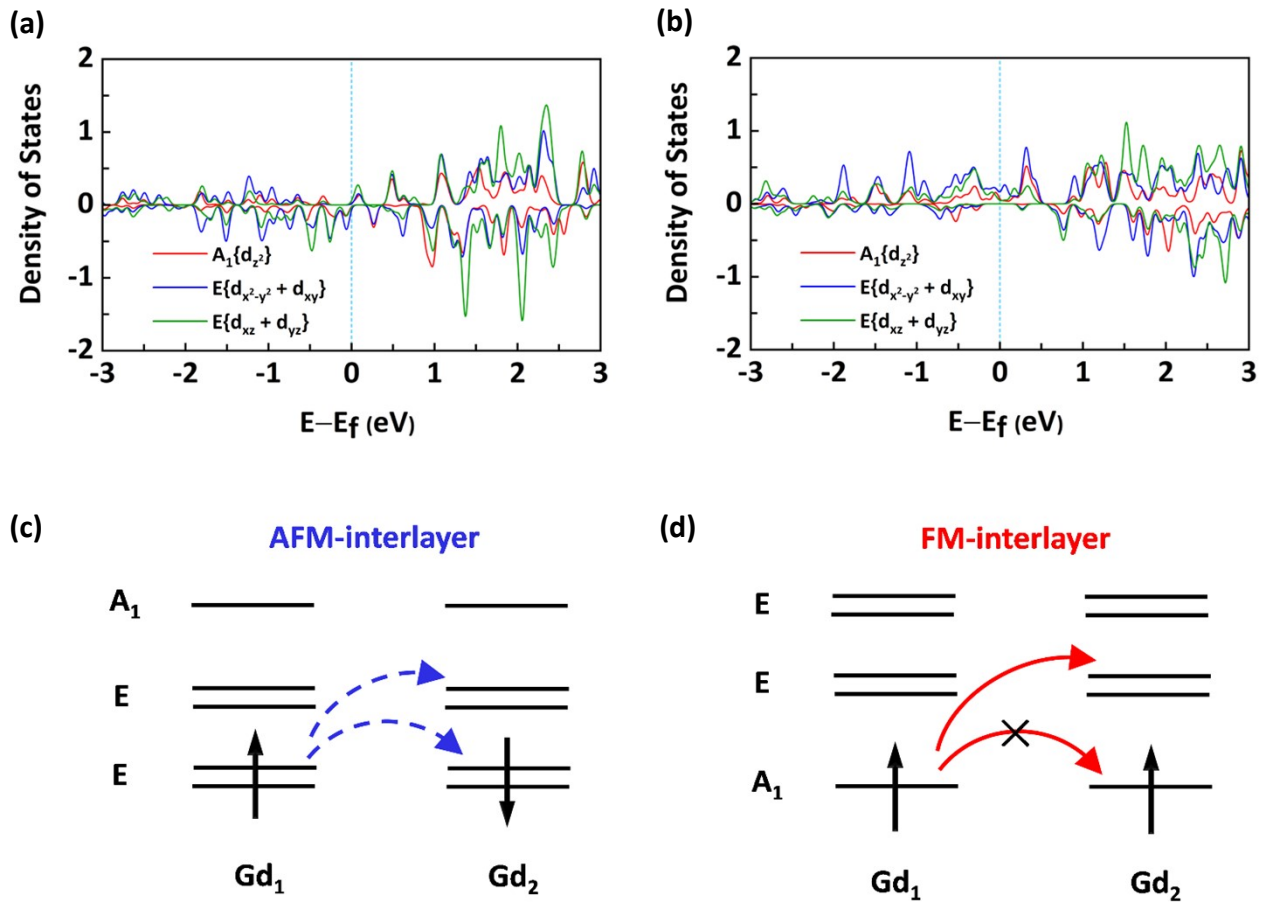


**Figure S12.** Orbital-resolved projected density of states of Gd atom in (a) AA-stacking and (b) AB-stacking bilayer GdGe<sub>2</sub> calculated by HSE06 method, respectively. (c) and (d) Schematic diagram showing the hopping mechanism of Gd-5d electrons for anti-ferromagnetic (AFM) and ferromagnetic (FM) interlayer exchange interactions, respectively.

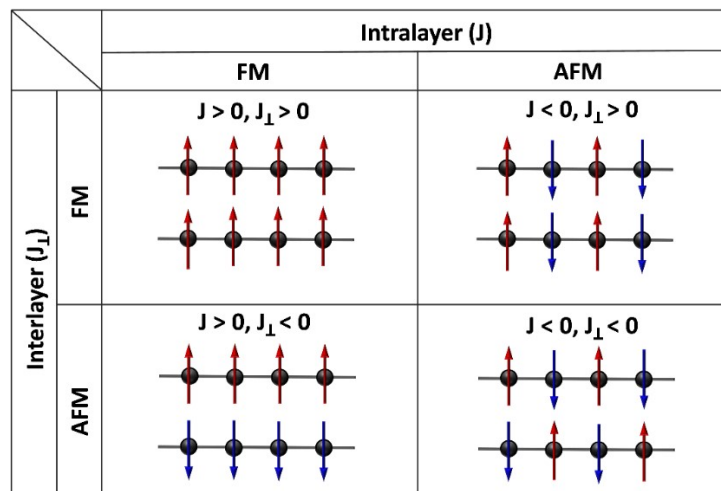


**Figure S13.** Schematic diagram showing the four magnetic configurations of bilayer GdGe<sub>2</sub> with considering the intralayer and interlayer magnetic couplings.

Considering with the interlayer nearest neighboring (NN) and second NN (2NN) magnetic couplings, the spin-Hamiltonian of the bilayer GdGe<sub>2</sub> is calculated as:

$$H = - \sum_{nm} J \vec{S}_n \cdot \vec{S}_m - \sum_{ij} J_{1\perp} \vec{S}_i \cdot \vec{S}_j - \sum_{ik} J_{2\perp} \vec{S}_i \cdot \vec{S}_k \quad (1)$$

where  $J$  is the intralayer NN magnetic coupling paramant,  $J_{1\perp}$  and  $J_{2\perp}$  represent the interlayer NN and 2NN magnetic coupling paramants, respectively. Four magnetic configurations shown in Figure S11 for AA-stacking and AB-stacking bilayer GdGe<sub>2</sub> have been calculated and their energies are described as equation (2) and (3), respectively.

$$\begin{aligned} E_{FM}^{FM} &= E_0 - 24J \cdot |S|^2 - 4J_{1\perp} \cdot |S|^2 - 24J_{2\perp} \cdot |S|^2 \\ E_{FM}^{AFM} &= E_0 - 24J \cdot |S|^2 + 4J_{1\perp} \cdot |S|^2 + 24J_{2\perp} \cdot |S|^2 \end{aligned} \quad (2)$$

$$\begin{aligned} E_{AFM}^{FM} &= E_0 + 8J \cdot |S|^2 - 4J_{1\perp} \cdot |S|^2 + 8J_{2\perp} \cdot |S|^2 \\ E_{AFM}^{AFM} &= E_0 + 8J \cdot |S|^2 + 4J_{1\perp} \cdot |S|^2 - 8J_{2\perp} \cdot |S|^2 \end{aligned}$$

$$\begin{aligned} E_{FM}^{FM} &= E_0 - 24J \cdot |S|^2 - 12J'_{1\perp} \cdot |S|^2 - 12J'_{2\perp} \cdot |S|^2 \\ E_{FM}^{AFM} &= E_0 - 24J \cdot |S|^2 + 12J'_{1\perp} \cdot |S|^2 + 12J'_{2\perp} \cdot |S|^2 \end{aligned} \quad (3)$$

$$E_{AFM}^{FM} = E_0 + 8J \cdot |S|^2 + 4J'_{1\perp} \cdot |S|^2 - 12J'_{2\perp} \cdot |S|^2$$

$$E_{AFM}^{AFM} = E_0 + 8J \cdot |S|^2 - 4J'_{1\perp} \cdot |S|^2 + 12J'_{2\perp} \cdot |S|^2$$

$E_0$  means the ground state energy of nonmagnetic state, superscript and subscript represent the type of interlayer and intralayer magnetic couplings, respectively.  $S$  is the spin vector of magnetic atoms. The calculated magnetic coupling paramants were summarized in Table S1.

**Table S1.** Magnetic ground state, magnetic coupling parameters of intralayer and interlayer exchange interactions in AA-stacking and AB-stacking bilayer GdGe<sub>2</sub>.  $J$  is the magnetic coupling parameter between intralayer nearest neighboring (NN) Gd atoms,  $J_{1\perp}$  and  $J_{2\perp}$  represent the magnetic coupling parameters between the interlayer NN and second NN (2NN) Gd atoms, respectively.

	Ground state	$J$ (meV)	$J_{1\perp}$ (meV)	$J_{2\perp}$ (meV)
AA-stacking	AFM	0.389	-0.054	-0.022
AB-stacking	FM	1.041	0.495	0.198

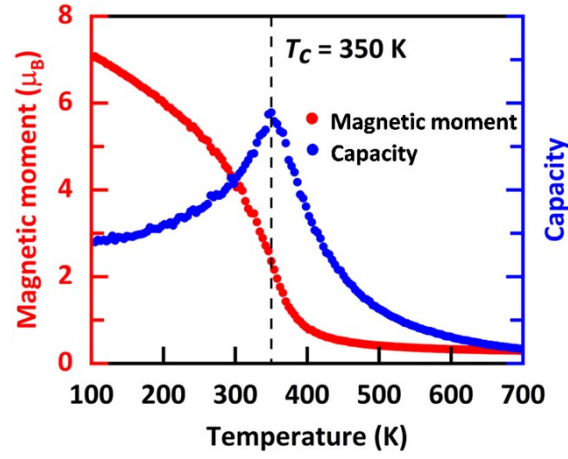


**Figure S14.** The evolution of magnetic moment of Gd atom (red) and specific heat (blue) with respect to temperature for AB-stacking bilayer GdGe<sub>2</sub>.